ELSEVIER

Journal of Nuclear Materials 252 (1998) 135–144

journal of nuclear materials

Carbon deposition from a γ-irradiated $CO_2/CO/CH_4/C_2H_6$ gas mixture on magnetite Fe_3O_4

G.C. Allen *, K.R. Hallam

University of Bristol, Interface Analysis Centre, 121 St. Michael's Hill, Bristol BS2 8BS, UK

Received 30 April 1996; accepted 27 August 1997

Abstract

Previous studies have indicated that carbon is deposited on spinel-type oxides containing manganese, iron, nickel and chromium manganese oxides and uranium oxides, especially where rapid electron exchange is possible in mixed valence compounds. In this investigation, characterised magnetite, Fe_3O_4, surfaces have been subjected to γ-irradiation under conditions of temperature, pressure and atmosphere similar to those experienced in reactor with the aim of furthering our understanding of the catalytic processes involved in deposit initiation and growth. Although it was not possible to produce large (111) Fe_3O_4 planes, enhanced carbon deposition was observed on small (111) regions showing the enhanced catalytic effect of these planes for carbon deposition out of the gas phase. © 1998 Elsevier Science B.V.

1. Introduction

Carbon deposition has been observed in power reactors on surfaces used in reheater and superheater pipework under operating conditions. Such deposition results in a reduction in heat-transfer efficiency and may require down rating of the reactor to prevent overheating of the fuel. Two probable sources of the carbon deposit are methane and carbon monoxide, which are added to the carbon dioxide gas coolant to reduce the radiolytic oxidation of the graphite moderator.

Previous studies [1,2] have shown that nickel–iron or magnetite surfaces catalyse the decomposition of CH and CHO species, such as ethyne or propanone, producing filamentary carbon. The coolant is stable in the absence of radiation, but in reactor, radiolysis of the gas produces several deposition precursors which may be catalytically decomposed to give carbon [3].

Baker et al. [1] studied the effect of the surface state of iron on carbon deposition and found that FeO was superior to metallic iron as an active catalyst for filamentous carbon formation. This increased activity arose as the FeO was able to decompose to form a high surface area iron catalyst in situ. Other workers, such as Galuszka and Back [4], found that iron surfaces which had undergone oxidation–reduction treatment decomposed methane to give filamentous carbon, but that untreated iron did not. Again, the treatment of the sample prior to exposure to a carbon-depositing gas mixture lead to fragmentation of the surface, creating iron fragments of a suitable size for filamentary carbon growth. Without this surface disruption, no carbon filaments were produced.

Lambiev and Dimitrov [5] looked at the reduction kinetics of Fe_2O_3 and Fe_3O_4 in CO at temperatures of 300–1000°C. The synthetic Fe_2O_3 had a mean grain size, before reaction, of 1–2 μm while the natural Fe_3O_4 had grains some ten times larger (20–30 μm mean size). Carbon deposition on Fe_2O_3 was seen to occur, maximising at a temperature of 500°C. Fe_3O_4, likewise, showed deposition. It is likely that this deposition occurred on the metallic iron formed in the samples. In comparison to those produced off FeO, the filaments generated by Fe_3O_4 were fewer in number but wider.

Lund at al. [6] reviewed studies of the water gas shift reaction ($CO + H_2O \rightleftarrows CO_2 + H_2$) catalysed by magnetite, Fe_3O_4. The reaction was seen to occur via repeated

* Corresponding author. Tel.: +44-117 925 5666; fax: +44-117 925 5646; e-mail: g.c.allen@bristol.ac.uk.

PII S0022-3115(97)00276-6

oxidation and reduction of the 10% of the catalyst surface that was active. The octahedral Fe(II) and Fe(III) cations, with their rapid electron exchange, would appear to be the favoured location for this regenerative reaction to occur. Coordinatively unsaturated cations provided the adsorption sites for the CO, which acts to reduce anion sites. Steam oxidises the resulting oxygen vacancies to regenerate the catalyst. CO_2 adsorption was associated with surface oxygen species.

To identify the role played by mixed valency and rapid electron exchange, the extent of carbon deposition has been studied for spinel surfaces, uranium oxide and manganese oxide [7,8]. It has been suggested that Fe^{2+}/Fe^{3+} sites on the surface of iron-containing spinels catalyse the formation of dense carbon deposits.

To verify the above suggestions regarding the importance of electron transfer in carbon deposition, the effect of various magnetite surfaces on the rate of carbon deposition was investigated. Compared to the small grain size samples in the studies summarised above [1,4,5], we have attempted to use large single crystal samples to study reaction on various crystallographic planes.

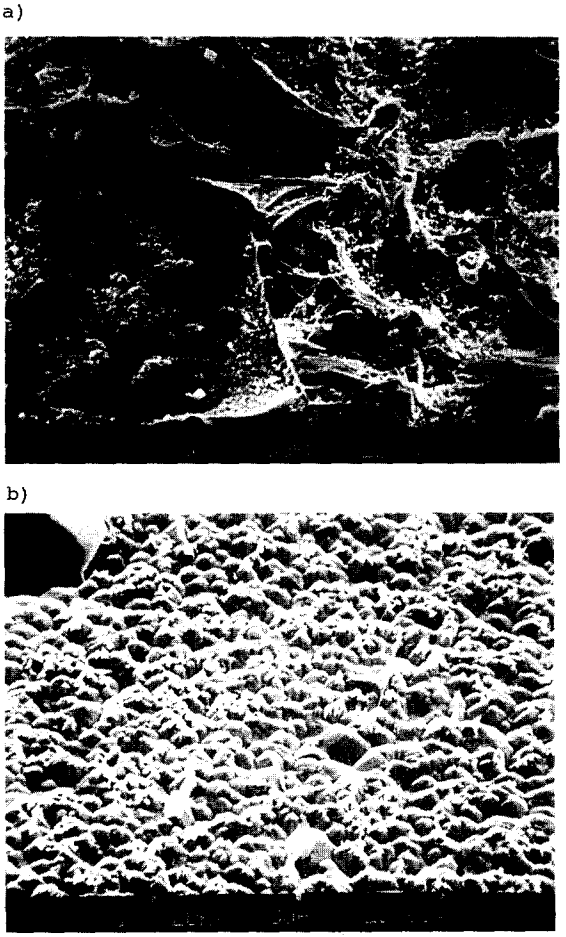

Fig. 1. Scanning electron micrographs of a (100) magnetite slice: (a) before, and (b) after 30 min non-ultrasonic etch in 12 M $HCl_{(aq)}$.

Fig. 2. Scanning electron micrograph of a (100) magnetite slice after 30 min non-ultrasonic etch in 12 M $HCl_{(aq)}$, edge region.

2. Experimental

2.1. Magnetite, Fe_3O_4, preparation

After ultrasonic cleaning in propan-2-ol, magnetite crystals were mounted in cold setting resin (Buehler SW). A diamond cutting wheel was used to slice the crystals parallel to the three principal planes, (100), (110), and (111). The 1.5 mm thick slices were then polished to 1/4 μm with graded silicon carbide papers and diamond pastes. Oil based lubricants were used for these operations to minimise oxidation of the sample surfaces. After removal of the mounting medium, the prepared slices were given another ultrasonic clean before examination and subsequent exposure in the gamma cell. X-ray diffractometry was used to confirm the orientation of these slices to within 5°.

While some magnetite slices were exposed in the gamma cell in the polished state, a selection of etching solutions were investigated to see if it was possible to improve the desired crystallographic planes.

2.2. The (100) magnetite surface

Crystals cut to reveal the (100) surface were exposed in an ultrasonic bath to 0.5 M oxalic acid for periods of up to 240 min. The surfaces became generally rougher but there was no sign of preferential etching in any direction. Immersion in 12 M $HCl_{(aq)}$ for 30 min gave more selective dissolution and created eight sided dimples on the surface (Fig. 1). At the edges of the slices, the dimples could be seen to be oriented parallel to the smoothed and triangular pitted (111) faces (Fig. 2). Shorter etch periods formed

Fig. 3. Scanning electron micrograph of a (110) magnetite slice after 240 min non ultrasonic etch in 0.5 M oxalic acid.

proportionally fewer dimples at the surface. The use of an ultrasonic bath allowed shorter etch times to be used for the same effect. In all cases, the solution became yellow as Fe^{3+} ions were released into solution.

2.3. The (110) magnetite surface

Crystals cut to reveal the (110) surface were exposed to 0.5 M oxalic acid in an ultrasonic bath. Initially an increase in surface roughness was observed which after longer exposure for 240 min left regions of the slice, between rough areas, covered in angular projections (Fig. 3). Exposure to 12 M HCl in an ultrasonic bath for $2\frac{1}{2}$ min produced a smooth uneven surface. Some slices had spines left proud of the surface (Fig. 4) which were shown by energy dispersive X-ray analysis to be titanium rich. These arose from non etching of impurities in the natural magnetite crystal.

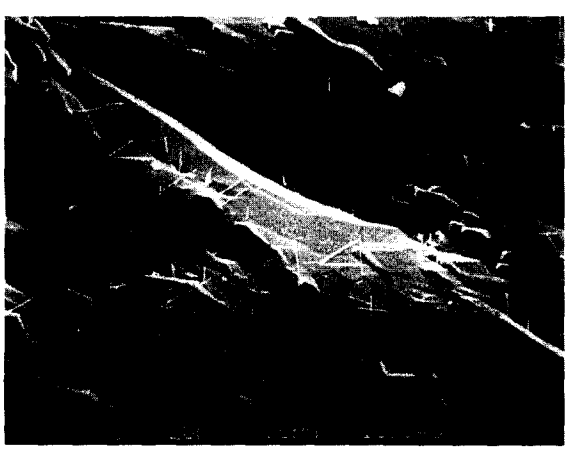

Fig. 4. Scanning electron micrograph of a (110) magnetite slice after $2\frac{1}{2}$ min ultrasonic etch in 12 M $HCl_{(aq)}$.

Fig. 5. Scanning electron micrograph of a (111) magnetite slice after 240 min ultrasonic etch in 0.5 M oxalic acid.

2.4. The (111) magnetite surface

The exposure of the (111) face of the magnetite crystal to 0.5 M oxalic acid in an ultrasonic bath roughened the surface. After longer etch times, some structure could be seen. Fig. 5 shows the surface of a slice after a total of 240 min etching. The formation of some triangular pits was observed on the rough surface. Etching (111) with 12 M $HCl_{(aq)}$ in an ultrasonic bath for 5 min produced triangular pits and pyramidal facets. The magnetite was more rapidly dissolved in cracked regions. Longer etch times degraded the surface, creating deep fissures and a rough surface. If an ultrasonic bath was not used, material removed from the bulk of the slice formed a skin over the surface of the crystalline sample. Lower acid concentrations increased the time required for the formation of a particular surface morphology. The (111) edges of (100) and (110) slices showed similar changes on etching to the larger (111) faces on the (111) slices. Solutions of 18 M $H_2SO_{4(aq)}$ and 0.1 M $Na_2H_2EDTA_{(aq)}$ had little effect on the surface of immersed specimens and no yellowing of the solution occurred.

Although it was not found possible to produce well defined crystallographic faces on the magnetite slices using the above etchants, it was decided to expose magnetite slices in the gamma cell that had been etched in an ultrasonic bath using 12 M $HCl_{(aq)}$ for periods of $2\frac{1}{2}$ and 5 min. Samples from each of the three orientations were prepared accordingly.

2.5. Energy dispersive X-ray analysis

SEM and EDX analysis was carried out using a Cambridge Instruments S150 Mk II scanning electron microscope fitted with a Kevex windowless detector X-ray analysis system. The extent of carbon deposition on each magnetite surface was assessed by measuring the carbon-

K_α X-ray peak count per 100 s. Quantitative analysis of light elements is difficult using EDX and suitable correction factors were not available for this work. No carbon was detected on unirradiated samples.

2.6. X-ray diffraction

Unit cell parameters were recorded using a Siemens D500 X-ray diffractometer with unfiltered Cu radiation and Siemens Diffrac500 software. A graphite crystal monochromator in the diffracted beam removed Cu-K_β, fluorescent and incoherently scattered radiation.

2.7. X-ray photoelectron spectroscopy

XPS analysis was carried out using a Kratos XSAM800 spectrometer. Al-K_α X-ray radiation was used, with the source operating at 300 W. Quantitative analysis and spectral interpretation was performed using Kratos DS800 software, which also controlled data acquisition. Wide scans (1000–0 eV binding energy) were recorded followed by more highly energy resolved regional spectra for the elements of interest.

2.8. Radiation experiments

The prepared magnetite crystals were loaded into a silica tube with silica spacers designed to allow unimpeded gas flow over the discs. The silica tube was then loaded into a stainless-steel capsule and placed in the γ-cell at Berkeley Centre. A ^{60}Co source is used in this facility. The capsule was placed in an outer irradiation position where a dose rate of 7–9 Gy s^{-1} was obtained [10].

2.8.1. Experiment 1: γ-cell exposure at 550°C

The magnetite samples were maintained at a temperature of 550°C for between 18 and 46 days in the γ-cell facility. Gas of composition CO_2/1% CO with 800 vpm CH_4 and 15 vpm C_2H_6 was allowed to flow through the

Table 1
Magnetite samples exposed in the gamma cell

Sample	Orientation	Treatment (polishing +)	Temperature (°C)	Time (days)
1.2.1[a]	(110)	none	550	18 + 28
1.2.2[a]	(110)	none	550	18 + 28
1.3[a]	(110)	none	550	18 + 28
1.4[a]	(110)	none	550	18 + 28
5.2	(100)	none	550	18 + 28
5.3	(100)	none	550	18 + 28
5.4	(100)	none	550	18 + 28
5.5	(100)	none	550	18 + 28
6.3	(111)	none	550	18 + 28
6.4	(111)	none	550	18 + 28
6.5	(111)	none	550	18 + 28
6.6	(111)	none	550	18 + 28
9.1	(100)	$2\frac{1}{2}$ min 12 M $HCl_{(aq)}$	550	22
9.2	(100)	5 min 12 M $HCl_{(aq)}$	550	22
9.3	(100)	$2\frac{1}{2}$ min 12 M $HCl_{(aq)}$	650	22
9.4	(100)	5 min 12 M $HCl_{(aq)}$	650	22
10.1	(111)	$2\frac{1}{2}$ min 12 M $HCl_{(aq)}$	550	22
10.2	(111)	5 min 12 M $HCl_{(aq)}$	550	22
10.3	(111)	$2\frac{1}{2}$ min 12 M $HCl_{(aq)}$	650	22
10.4	(111)	5 min 12 M $HCl_{(aq)}$	650	22
14.1	(110)	$2\frac{1}{2}$ min 12 M $HCl_{(aq)}$	550	22
14.2	(110)	5 min 12 M $HCl_{(aq)}$	550	22
14.3	(110)	$2\frac{1}{2}$ min 12 M $HCl_{(aq)}$	650	22
14.4	(110)	5 min 12 M $HCl_{(aq)}$	650	22
15.2	(110)	unpolished	650	24
15.3	(110)	unpolished	550	24
15.4.2	(110)	unpolished	550	24
15.5	(110)	unpolished	650	24
57.2	(111)	unpolished	550	23
57.5	(111)	unpolished	650	23
57.7.2	(111)	unpolished	550	23
57.8	(111)	unpolished	650	23

[a]Crystal number 1 contained Fe_2O_3 regions.

Table 2
Iron and oxygen ratios, as calculated from beryllium window EDX spectra of magnetite slices

Sample	Atomic ratios	
	Fe	O
5 (100)	3.31	3.69
6 (111)	3.34	3.66
15 (110)	3.07	3.93
22 (100)	3.00	4.00
24 (111)	2.98	4.02
57 (111)	3.17	3.83

capsule at a rate of 2–3 cm^3 min^{-1} and 40 bar pressure in a single-pass experiment (see Table 1).

2.8.2. Experiment 2: γ-cell exposure 650°C

The magnetite samples were maintained at 650°C for 22–24 days using the gas composition and flow conditions of experiment 1 (see Table 1).

3. Results

3.1. Characterisation of magnetite, Fe_3O_4 crystal surfaces

The magnetite single crystals used in this study were natural occurring specimens from W. Australia and obtained from Richard Taylor Minerals of Cobham, UK. They exhibited an octahedral habit and ranged in size from 0.5–1.5 cm across. Some showed Fe_2O_3 rich regions and others were too brittle to be cut into specific orientations. The importance of analysis of samples prior to exposure in the gamma cell was highlighted by the discovery that some of the octahedral crystals were in fact martite, and not magnetite, or a mixture of the two. Martite is a form of haematite, Fe_2O_3, and a pseudomorph of magnetite [9]. Examples were found among the crystals containing both magnetite and Fe_2O_3 regions. When such crystals were cut, the lubricant turned red in colour, instead of the usual black/grey found with genuine magnetite crystals. Cutting also tended to take longer with these crystals. The XRD spectrum from a polished (110) slice of a crystal containing Fe_2O_3 showed not only a set of (220), (440) and (660) peaks but also a series of Fe_2O_3 signals including a strong (300) peak (Fig. 6). (111) slices also gave XRD spectra containing both Fe_3O_4 and Fe_2O_3 contributions.

A banded structure was sometimes apparent, with magnetite strips in a martite matrix. Silica, SiO_2, inclusions were sometimes seen. EDX was used to calculate the oxygen content of a spectrum recorded from one of these inclusions. Silicon dioxide was identified to within 1 at% of the stoichiometric composition. Away from such inclusions, an iron:oxygen atomic percentage ratio of 1:1.27 was obtained. After eighteen days in the gamma cell at

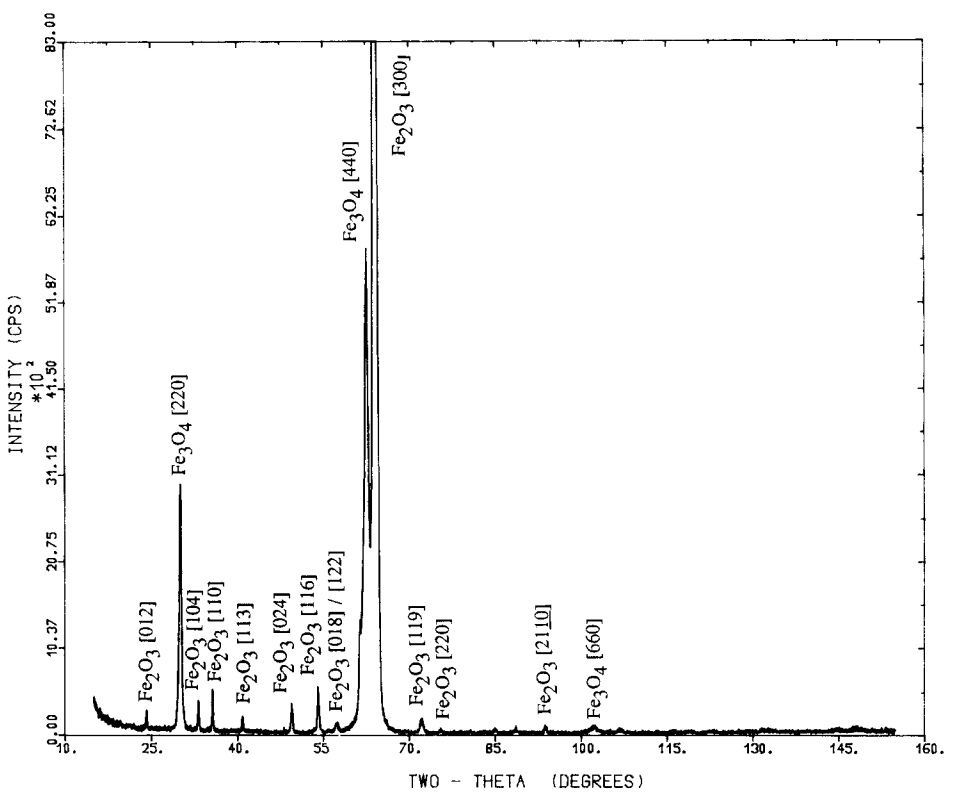

Fig. 6. XRD spectrum of a martite-containing (110) magnetite slice.

Table 3
Fe $2p_{3/2}$ XPS binding energy values obtained off Fe_3O_4 slices prior to gamma cell exposure

Sample	Binding energy (eV)			FWHM (eV)			Area ratio Fe(II):Fe(III)
	Fe $2p_{3/2}$	Fe(II) $2p_{3/2}$	Fe(III) $2p_{3/2}$	Fe $2p_{3/2}$	Fe(II) $2p_{3/2}$	Fe(III) $2p_{3/2}$	
5 (100)	710.5	709.5	711.0	4.3	3.3	3.7	1:1.46
6 (111)	710.3	709.2	710.9	4.3	3.3	3.6	1:1.86
9 (100)	–	709.0	711.0	–	3.1	4.2	1:3.10
10 (111)	–	709.5	711.3	–	3.5	3.8	1:1.48
14 (110)	–	709.4	711.2	–	3.3	3.8	1:1.98
15 (110)	–	709.0	711.1	–	3.4	4.0	1:1.86
22 (100)	–	709.3	711.3	–	3.4	3.9	1:1.45
57 (111)	–	709.3	711.2	–	3.5	4.0	1:1.35

550°C, an almost pure Fe_3O_4 XRD spectrum was obtained from one of these slices, showing the effect of the reducing conditions on the sample. An Fe:O atomic ratio of 1:12 was found using EDX and in the X-ray photoelectron spectrometer the Fe $2p_{3/2}$ peak shifted to lower binding energy.

3.2. Energy dispersive X-ray analysis of magnetite crystals

EDX spectra often showed the presence of titanium and vanadium impurities in the crystals at < 1 at% concentration. In some samples Al/Si/Ca, Mg/Al/Si, Ba/S and Mg/Al/Si/K particles were identified. After cutting, faces of the magnetite crystals were examined using the ZAF routines in the software to determine oxygen concentrations. Atomic percentages close to those expected for Fe_3O_4 were obtained. Polished samples often gave results high in iron and low in oxygen. Table 2 lists Fe:O ratios recorded from various magnetite samples.

3.3. X-ray diffraction

X-ray diffraction was used to characterise the crystal faces obtained by cutting the magnetite crystals. In each case the appropriate reflections were obtained from the crystal plane produced. Thus (100) slices gave peaks at the (400) and (800) positions, (110) slices gave (220, (440) and (660) reflections and for the (111) slices, (111), (222), (333), (444), (555) and (666) reflections were obtained. For the latter, it was noted that the signals generally peaked at the (333) position. With increasing gamma cell exposure, the peak intensity shifted to the (222) and (111) signals. The $K_{\alpha 2}$ X-ray contribution was more apparent at higher 2θ values.

3.4. X-ray photoelectron spectroscopy

Distinct Fe(II) peaks have been seen in XPS spectra of Fe_3O_4 [10]. This is explained in terms of the timescale of the XPS experiment in comparison to the time required for electron exchange.

The binding energy values recorded from the magnetite samples prior to gamma cell exposure are summarised in Table 5. In all cases, the peak shapes determined for Fe(II) and Fe(III) compounds were used to fit the Fe 2p signals. The overall Fe $2p_{2/3}$ peak envelopes measured in the present experiments were centred at 710.4 eV, a little lower than the average literature value of 710.9 eV referenced to the C 1s signal at 285.0 eV [10,11]. However, the Fe(II) and Fe(III) signals obtained by deconvolution agreed well with published values [12–16].

The polished (111) magnetite sample showed no change in binding energy after being left in a vacuum desiccator for several months, though the C 1s intensity increased at the expense of the other signals. Similarly, no change was noted upon leaving the sample in the spectrometer for four days, although an increase in hydrocarbon contamination occurred. XP spectra were recorded from a (110) sample before and after a 5 min etch in 12 M $HCl_{(aq)}$ (using an ultrasonic bath). A slight increase in intensity to the high binding energy side of the Fe $2p_{3/2}$ photoelectron peak was noted indicating an increase in the Fe(II):Fe(III) ratio from 1:1.98 to 1:2.73 [17]. The contributing Fe(II) and Fe(III) peaks were also broadened ($FWHM_{Fe(II)} = 3.4$ eV; $FWHM_{Fe(III)} = 4.3$ eV) and an increase in the high binding energy component of the O 1s peak indicated an increase in hydroxyl species at the surface of the sample [18].

3.5. Characterisation of magnetite after exposure in the γ-cell

3.5.1. Energy dispersive X-ray analysis

Most samples examined using the beryllium window EDX analyser showed some surface oxidation. For exam-

Table 4
Fe(II):Fe(III) XPS peak area ratios after gamma cell exposure

Sample	Area ratio Fe(II):Fe(III)
5 (100)	1:1.46
6 (111)	1:1.30
9 (100)	1:2.24

ple, the (100) crystal surface after exposure gave the formula $Fe_{3.02}O_{3.98}$ in which the oxygen concentration was calculated by difference. Before exposure, analysis of this sample by the same method gave the composition $Fe_{3.31}O_{3.69}$.

When the windowless EDX detector was used the exposed samples showed greater carbon signals in central regions. The edges were shielded from the gas mixture by silica spacers of the sample holder. Spectra were recorded from many different areas of the samples but the analyses were affected by the orientation of the area selected with respect to the X-ray detector and the line-of-sight path from the area selected. When looking at faces with a ready line-of-sight to the detector, carbon and oxygen signals were enhanced in comparison to spectra recorded from, for instance, inner walls of etch pits or large areas covering a range of surface topography. Low energy signals were much reduced in intensity in spectra recorded from faces directed away from the detector. Further evidence for this effect was obtained from polished samples which gave consistently greater count rates than the etched ones. The strong influence of topography on the EDX spectra acquired precluded the determination of relative deposition rates for different samples by this method.

Table 5
Fe:C atomic ratios for samples before and after exposure, derived from X-ray photoelectron spectra

Sample	State 1	Fe:C
5 (100)	before exposure	0.40:1
5.3	after exposure at 550°C	0.01:1
6 (111)	before exposure	0.29:1
6.3	after expsure at 550°C	0.01:1
9 (100)	before exposure	0.36:1
9.1	after exposure at 550°C	–
9.3	after exposure at 650°C	0.12:1
9.2	after exposure at 550°C	–
9.4	after exposure at 650°C	0.01:1
10 (111)	before exposure	0.63:1
10.1	after exposure at 550°C	–
10.3	after exposure at 650°C	0.01:1
10.2	after exposure at 550°C	–
10.4	after exposure at 650°C	0.02:1
14 (110)	before exposure	0.32:1
14.1	after exposure at 550°C	–
14.3	after exposure at 650°C	0.03:1
14.2	after exposure at 550°C	–
14.4	after exposure at 650°C	0.03:1
15 (110)	before exposure	0.19:1
15.3	after exposure at 550°C	–
15.2	after exposure at 650°C	0.02:1
57 (111)	before exposure	0.26:1
57.7.2	after exposure at 550°C	–
57.8	after exposure at 650°C	–

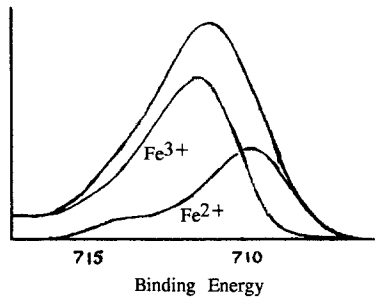

Fig. 7. An example of Fe $2p_{3/2}$ XPS peak fit (111) slice.

3.5.2. X-ray diffraction

After exposure in the gamma cell, the magnetite samples gave diffraction patterns with narrower peaks. The only difference in the diffraction peaks recorded from the (111) slice 57.7.2 after 23 days exposure in the gamma cell at 550°C, compared to that recorded before exposure, was the absence of Fe_2O_3 peaks, following reduction of haematite to magnetite in the gas conditions used. No peaks other than those due to Fe_3O_4, magnetite, were identified.

3.5.3. X-ray photoelectron spectroscopy (see also Tables 4 and 5)

All X-ray photoelectron spectra recorded after exposure of a sample in the gamma cell showed much reduced Fe 2p photoelectron signals, a consequence of covering the sample surfaces with a layer of carbon. These features were also much broader than those recorded before exposure but their positions had changed little. Fig. 8 compares the wide scan spectra from a (111) crystalline sample before and after exposure for 18 days at 550°C. A change in the C 1s photoelectron signal is evident. In general the C 1s peak recorded from polished samples at 284.6 eV was narrower than that from 'adventitious' carbon observed before exposure.

4. Discussion

Magnetite oriented in the (111) direction is able to present close packed arrays of octahedrally coordinated ions to the gas phase. Thus, Fe(II)/Fe(III) couples are available to freely interact with gas phase species. (100) and (110) faces only present the edges of the Fe(II)/Fe(III) planes. We might, therefore, anticipate seeing more rapid carbon deposition on samples cut to expose (111) planes than on those sliced to reveal (100) or (110) planes. Magnetite, in the form of a pressed powder pellet, was shown in an earlier study to produce filamentous carbon deposition when exposed in the gamma cell at 650°C [19].

We set out in this work to see if it was possible to detect differences in deposition rate on different crystallographic faces of large magnetite single crystals.

The task of preparing the desired crystallographically smooth magnetite surfaces was a difficult one. Some smooth surfaces and regular etch patterns were obtained, although these were rarely continuous over the prepared crystal face. To compound the problem, large topographical influences on the relative intensities of the detected EDX signals were encountered. Effort was concentrated, therefore, on topographically smooth and oriented regions of the various faces obtained.

No filamentary carbon deposition was identified on any of the magnetite samples exposed in the gamma cell. This contrasts with the results obtained from pressed powder pellet samples of Fe_3O_4 [19] but can be explained by the reduced ability of the sample to produce iron particles of the correct size to initiate filamentary carbon deposition. It

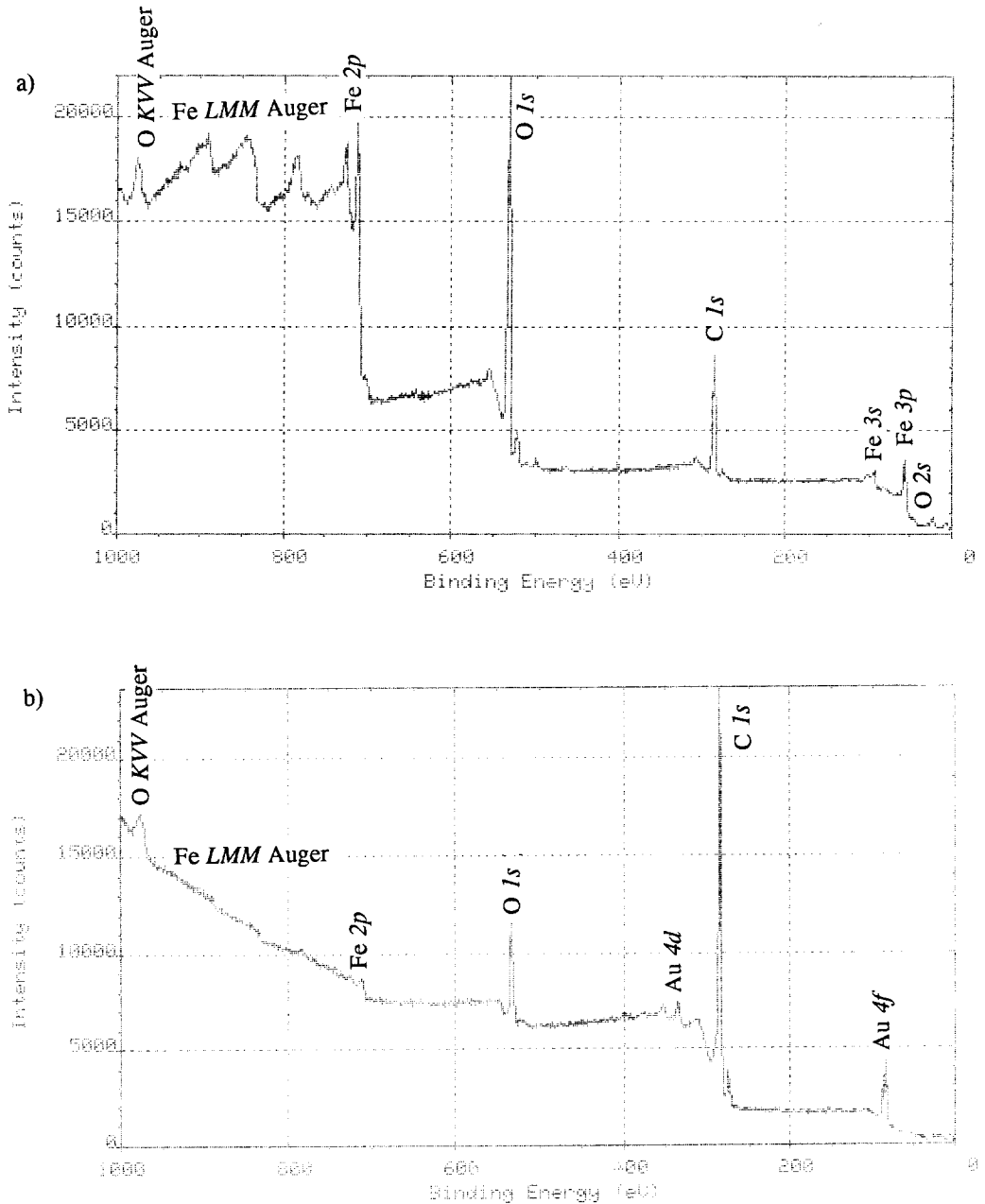

Fig. 8. XPS spectra of (111) magnetite slice 6.3: (a) before, and (b) after 18 days at 650°C.

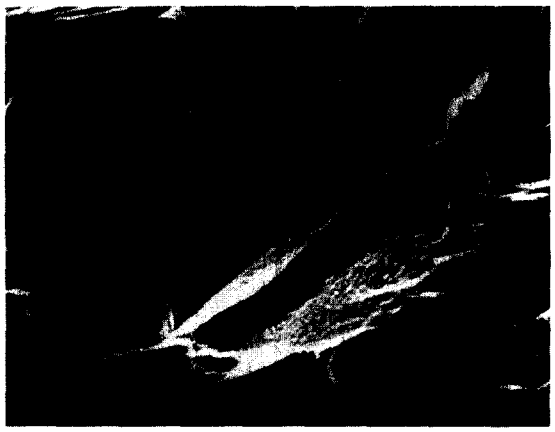

Fig. 9. Scanning electron micrograph of (110) magnetite slice ($2\frac{1}{2}$ min 12 M $HCl_{(aq)}$) 14.3 after 22 days at 650°C.

would appear that any iron produced by reduction of the Fe_3O_4 remains firmly bound to the sample surface. Edge (shielded from the gas phase by the silica spacers) and central regions of the slices were identified, either visually or using scanning electron microscopy. This, together with the presence of carbon signals in the EDX and XP spectra, suggested that carbon was deposited in a smooth blanket form across the crystal faces. Two samples, etched and exposed at 650°C, showed some regions where structure was present in the deposition material. One of these samples was a (111) crystal and the structure was apparent on a flat etched face approximately parallel to the (111) plane. The other slice showing such a surface feature was originally cut parallel to the (110) direction, but the deposit was present on a face at an angle to this (Figs. 8 and 9). The (111) plane of magnetite has previously been shown to be the most rapidly etched of the (100), (110) and (111) planes [18], and it was expected that this face would give the greater amount of carbon deposition. It is able to present to the gas phase large arrays of octahedrally coordinated Fe^{2+} and Fe^{3+} ions, able to rapidly exchange electrons and interact with gas phase hydrocarbon radicals.

Norfolk et al. [3] showed that the main deposit precursor in irradiated gas systems of the type used here is C_2H_4, which undergoes radiolysis to form $C_2H_3^{\cdot}$ radicals. Mechanisms for the deposition on magnetite surfaces could include an initiation step resulting in the formation of a π-bond between a $C_2H_3^{\cdot}$ radical and an octahedrally coordinated Fe^{II}/Fe^{III} site at the surface through which electron transfer may occur (Fig. 10). Propagation of a carbon

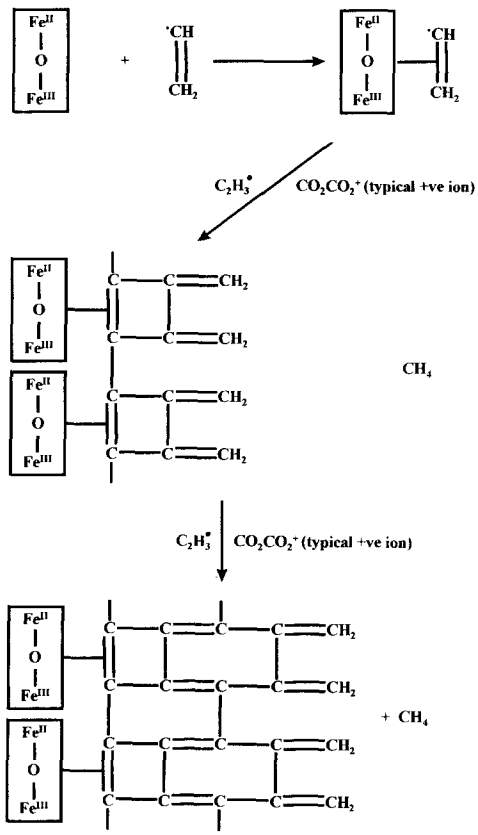

Fig. 10. Carbon growth initiated at Fe^{II}/Fe^{III} site by π-bonding with hydrocarbon radicals (typically $C_2H_3^{\cdot}$).

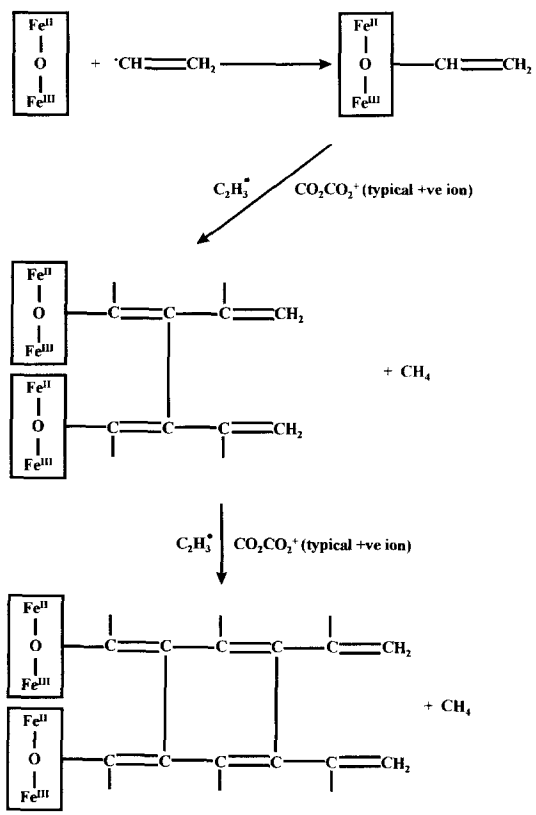

Fig. 11. Carbon growth initiated at Mn^{II}/Mn^{III} site by σ-bonding with hydrocarbon radicals (typically $C_2H_3^{\cdot}$).

chain follows via the abstraction of hydrogen atoms from the surface complex by positive ions such as $CO_2CO_2^+$ in the irradiated gas mixture [2]. Alternatively the initiation stop may involve the formation of a σ-bond between the unpaired electron on a $C_2H_3^{\cdot}$ radical and a surface Fe^{II}/Fe^{III} site (Fig. 11). These mechanisms would be expected to leave the catalytic site embedded in the iron oxide surface, producing the thin, dense carbon deposit layers observed in this study.

The appearance of carbon deposits on faces of approximately (111) orientation indicates preferential deposition on the (111) face of the single crystal magnetite. Although it proved impossible to prepare a perfect (111) plane which could be presented to the gaseous environment, local areas clearly identified as (111) were found to produce enhanced deposition. For a quantitative study of the deposition phenomenon it would be necessary to prepare larger surfaces of uniform orientation.

5. Conclusions

Perfectly selected Fe_3O_4 crystallographic planes could not be prepared but filamentary deposition was not observed on the magnetite slices. However a thin, dense carbon deposit was formed on all samples.

Structured deposit was seen on two smooth magnetite faces, including one oriented approximately parallel to the (111) direction. This face clearly produced enhanced carbon deposition, owing to its close packed arrays of interacting Fe^{2+} and Fe^{3+} ions.

Acknowledgements

The authors would like to thank Magnox Electric, Berkeley Centre and the Council for National Academic Awards for their support during the course of this work.

References

[1] R.T.K. Baker, R.J. Alonso, J.A. Dumesic, D.J.C. Yates, J. Catal. 77 (1982) 74.
[2] R.T.K. Baker, J.J. Chludzinski, J. Catal. 64 (1980) 464.
[3] D.J. Norfolk, R.F. Skinner, W.J. Williams, Proc. Conf. on Gas Chemistry in Nuclear Reactors and Large Industrial Plants, University of Salford, UK, Apr. 1980.
[4] J. Galuszka, M.H. Back, Carbon 22 (1984) 141.
[5] D.K. Lambiev, D.G. Dimitrov, CR Acad. Bulg. Sci. 20 (1967) 919.
[6] C.R.F. Lund, J.E. Kubsh, J.A. Dumesic, in: R.K. Grasselli, J.F. Brazdil (Eds.), Solid State Chemistry in Catalysis, American Chemical Society, 1985, p. 313.
[7] G.C. Allen, J.A. Jutson, J. Chem. Soc. Faraday Trans. I 85 (1989) 55.
[8] G.C. Allen, K.R. Hallam, J. Mater. Chem. 5 (1995) 1451.
[9] C.S. Hurlbut Jr., Dana's Manual of Mineralogy, 18th ed., Wiley, New York.
[10] G.C. Allen, P.M. Tucker, R. K Wild, Philos. Mag. B 46 (1982) 411.
[11] P. Mills, J.L. Sullivan, J. Phys. D 16 (1983) 723.
[12] K. Hirokawa, M. Oku, Talanta 26 (1979) 855.
[13] N.S. McIntyre, D.G. Zetaruk, Analyt. Chem. 49 (1977) 1521.
[14] K. Asami, K. Hashimoto, S. Shimodaira, Corros. Sci. 16 (1976) 35.
[15] C.R. Brundle, T.J. Chuang, K. Wandelt, Surf. Sci. 68 (1977) 459.
[16] K. Wandelt, Surf. Sci. Reports 2 (1982) 1.
[17] G.C. Allen, R.M. Sellers, P.M. Tucker, Philos. Mag. B 48 (1983) L4.
[18] G.C. Allen, C. Kirby, R.M. Sellers, J. Chem. Soc. Faraday Trans. I 84 (1988) 355.
[19] J.A. Jutson, The Deposition of Carbon on Transition Metal Oxide Surfaces, Council for National Academic Awards, PhD thesis, 1989.